



# New Nocobactin Derivatives with Antimuscarinic Activity, Terpenibactins A–C, Revealed by Genome Mining of *Nocardia terpenica* IFM 0406

Julia Chen,<sup>[a, b]</sup> Andri Frediansyah,<sup>[a, b, c]</sup> Daniel Männle,<sup>[a, b, d]</sup> Jan Straetener,<sup>[b, e]</sup> Heike Brötz-Oesterhelt,<sup>[b, e]</sup> Nadine Ziemert,<sup>[b, d]</sup> Leonard Kaysser,<sup>[a, b]</sup> and Harald Gross<sup>\*[a, b]</sup>

We report a genomics-guided exploration of the metabolic potential of the brasilicardin producer strain *Nocardia terpenica* IFM 0406. Bioinformatics analysis of the whole genome sequence revealed the presence of a biosynthetic gene cluster presumably responsible for the generation of formerly unknown nocobactin derivatives. Mass spectrometry-assisted isolation led

to the identification of three new siderophores, terpenibactins A (1), B (2) and C (3), which belong to the class of nocobactins. Their structures were elucidated by employing spectroscopic techniques. Compounds 1–3 demonstrated inhibitory activity towards the muscarinic M3 receptor, while exhibiting only a low cytotoxicity.

## Introduction

In the past, bacteria of the genus *Nocardia* were principally associated with a pathogenic context, having been described in 1888 by Edwin Nocard<sup>[1]</sup> as the causative agent of severe infections of the skin, lungs or the central nervous system in humans and animals.<sup>[2,3]</sup> However, within the last two decades, it has become apparent that this genus also possesses a tremendous biotechnological and pharmaceutical potential, with species that produce numerous versatile enzymes<sup>[4–6]</sup> and structurally novel and highly bioactive small molecules.<sup>[7,8]</sup> This

observation is also supported by analyses of the ever-increasing amount of publicly available *Nocardia* genome sequencing data.<sup>[9–12]</sup> Commonly, *Nocardia* spp. genomes comprise 16 to 49 biosynthetic gene clusters, which is why *Nocardia* spp. are considered ‘biosynthetically talented’ producers.

A prime example of such is the strain *Nocardia terpenica* IFM 0406 (formerly referred to as *Nocardia brasiliensis* IFM 0406).<sup>[13]</sup> It is known to produce the anti-staphylococcal lipolanthine nocavionin,<sup>[14]</sup> the antifungal brasilinolides<sup>[15–17]</sup> and the immunosuppressive brasilicardins.<sup>[18–21]</sup> In order to develop a safe biotechnological production platform for brasilicardins, we recently revisited this strain and reinvestigated the corresponding biosynthetic gene cluster, reported by Dairi and co-workers.<sup>[22]</sup> Within the framework of this study, we sequenced the whole genome of IFM 0406,<sup>[23]</sup> were able to redefine the borders of the gene cluster and achieved the heterologous expression of brasilicardin C.<sup>[24]</sup> Further analysis of the whole genome sequence indicated a gene cluster encoding a new nocobactin-like compound.

Structurally, nocobactins feature a C-terminal *N*-OH-cyclo-lysine bound to a long chain 3-OH fatty acid, whose hydroxy group is esterified by *N*<sup>ε</sup>-acyl-*N*<sup>ε</sup>-hydroxy-L-lysine. The  $\alpha$ -amino group of lysine is in turn linked to a 2-OH-phenyl-5-methyl-oxazole moiety. To date, a series of differently substituted congeners has been isolated from *Nocardia* species,<sup>[25–30]</sup> showing variation in the substitution pattern of the 2-OH-phenyl residue, of the oxazole ring system and of the  $\epsilon$ -nitrogen atoms of both lysine residues, or in the nature of the fatty acid (Table 1).

In this study, we describe the *in silico* identification of a new nocobactin biosynthetic gene cluster. Subsequently, the isolation, structure elucidation and biological evaluation of the resultant compounds, which we termed terpenibactins A–C, is presented.


[a] J. Chen, A. Frediansyah, D. Männle, Dr. L. Kaysser, Prof. Dr. H. Gross  
 Pharmaceutical Institute, Dept. of Pharmaceutical Biology  
 University of Tübingen  
 Auf der Morgenstelle 8, 72076 Tübingen (Germany)  
 E-mail: harald.gross@uni-tuebingen.de


[b] J. Chen, A. Frediansyah, D. Männle, J. Straetener, Prof. Dr. H. Brötz-Oesterhelt, Prof. Dr. N. Ziemert, Dr. L. Kaysser, Prof. Dr. H. Gross  
 German Center for Infection Research (DZIF)  
 Partner site Tübingen, 72076 Tübingen (Germany)


[c] A. Frediansyah  
 Research Division for Natural Product Technology (BPTBA)  
 Indonesian Institute of Sciences (LIPI), Wonosari 55861 (Indonesia)

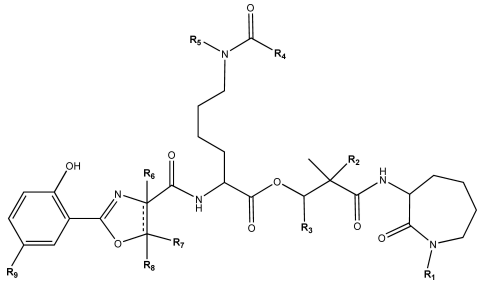
[d] D. Männle, Prof. Dr. N. Ziemert  
 Department of Applied Natural Products Genome Mining  
 Interfaculty Institute of Microbiology and Infection Medicine (IMIT)  
 University of Tübingen  
 Auf der Morgenstelle 28, 72076 Tübingen (Germany)

[e] J. Straetener, Prof. Dr. H. Brötz-Oesterhelt  
 Department of Microbial Bioactive Compounds  
 Interfaculty Institute of Microbiology and Infection Medicine (IMIT)  
 University of Tübingen  
 Auf der Morgenstelle 28, 72076 Tübingen (Germany)

 Supporting information for this article is available on the WWW under <https://doi.org/10.1002/cbic.202000062>

 This article is part of a Special Collection on Microbial Biosynthesis and Interactions. To view the complete collection, visit our homepage

 © 2020 The Authors. Published by Wiley-VCH Verlag GmbH & Co. KGaA. This is an open access article under the terms of the Creative Commons Attribution Non-Commercial NoDerivs License, which permits use and distribution in any medium, provided the original work is properly cited, the use is non-commercial and no modifications or adaptations are made.

**Table 1.** The nocobactin compound family.


Compound	R <sup>1</sup>	R <sup>2</sup>	R <sup>3</sup>	R <sup>4</sup>	R <sup>5</sup>	R <sup>6</sup>	R <sup>7</sup>	R <sup>8</sup>	R <sup>9</sup>	<i>m/z</i>	Ref.
nocobactin NA-a	OH	H	C <sub>9</sub> H <sub>19</sub>	CH <sub>3</sub>	OH	–	CH <sub>3</sub>	–	H	743.4	[25]
nocobactin NA-b	OH	H	C <sub>11</sub> H <sub>23</sub>	CH <sub>3</sub>	OH	–	CH <sub>3</sub>	–	H	771.4	[25]
formobactin	OH	CH <sub>3</sub>	C <sub>9</sub> H <sub>19</sub>	H	OH	–	CH <sub>3</sub>	–	H	743.4	[26]
amamistatin A	OH	CH <sub>3</sub>	C <sub>7</sub> H <sub>15</sub>	H	OH	–	CH <sub>3</sub>	–	OCH <sub>3</sub>	745.4	[27]
amamistatin B	H	CH <sub>3</sub>	C <sub>7</sub> H <sub>15</sub>	H	H	–	CH <sub>3</sub>	–	OCH <sub>3</sub>	713.4	[27]
brasilibactin A	OH	H	C <sub>15</sub> H <sub>31</sub>	H	OH	H	H	H	H	801.5	[28]
nocardimicin A	OH	H	C <sub>9</sub> H <sub>19</sub>	CH <sub>3</sub>	OH	–	H	–	H	729.4	[29]
nocardimicin B	OH	H	C <sub>11</sub> H <sub>23</sub>	CH <sub>3</sub>	OH	–	H	–	H	757.4	[29]
nocardimicin C	H	H	C <sub>11</sub> H <sub>23</sub>	CH <sub>3</sub>	OH	–	H	–	H	741.4	[29]
nocardimicin D	OH	H	C <sub>13</sub> H <sub>27</sub>	CH <sub>3</sub>	OH	–	H	–	H	785.5	[29]
nocardimicin E	H	H	C <sub>13</sub> H <sub>27</sub>	CH <sub>3</sub>	OH	–	H	–	H	769.5	[29]
nocardimicin F	OH	H	C <sub>15</sub> H <sub>31</sub>	CH <sub>3</sub>	OH	–	H	–	H	813.5	[29]
nocardimicin G	OH	H	C <sub>13</sub> H <sub>27</sub>	H	OH	H	H	H	H	773.5	[30]
nocardimicin H	OH	H	C <sub>15</sub> H <sub>31</sub>	H	OH	H	H	H	H	801.5	[30]
nocardimicin I	OH	H	C <sub>17</sub> H <sub>35</sub>	H	OH	H	H	H	H	829.5	[30]
predicted cpd.	OH	H	C <sub>7</sub> H <sub>15</sub> –C <sub>17</sub> H <sub>35</sub>	H	OH	H	CH <sub>3</sub>	H	H	703–844	this study

## Results and Discussion

### Identification and organization of the terpenibactin (*ter*) biosynthetic gene cluster

*In silico* whole genome sequence analysis of *N. terpenica* IFM 0406 using the bioinformatics web-tool antiSMASH 5.1.0<sup>[31]</sup> revealed the presence of 38 biosynthetic gene clusters (BGCs). Besides the readily identifiable known BGCs coding for nocavionin,<sup>[14]</sup> brasilinolide,<sup>[17]</sup> brasilicardin,<sup>[23,24]</sup> and ectoine,<sup>[32]</sup> two NRPS-PKS hybrid-based BGCs, both located on contig\_9 (accession no. LWGR01000021.1), were postulated to direct the biosynthesis of a nocobactin/mycobactin-like siderophore. Closer inspection of this BGC showed that it extensively parallels the nocobactin NA cluster.<sup>[33]</sup> Both share nine homologous genes out of ten genes in total and both are divided into two sub-gene clusters (sub-gene cluster 1 and 2). In the case of the *ter* gene cluster, the inter-subcluster region spans 282 kb (Figure 1). Slight differences exist in the fact that the NRPS *nbtF* homologue *terF* is located in sub-gene cluster 2 as opposed to sub-gene cluster 1, and instead of a lysine acetyltransferase similar to NbtH, the corresponding gene *terH* codes for a lysine formyltransferase that is located at the equivalent position in cluster one (Figure 1).

Having identified the split BGC, we predicted the resultant biosynthetic route.<sup>[33]</sup> Salicylate is synthesised from chorismate by the salicylate synthase TerS and activated by the salicylate-AMP ligase TerT, being tethered to the aryl carrier protein (ArCP) domain on the nonribosomal peptide synthetase (NRPS) TerF (Figure 2).

Here, threonine is also activated and cyclised, giving either 2-hydroxyphenyl-5-methyloxazoline or 2-hydroxyphenyl-5-methyloxazole. Recently, the candidate gene *sagB*, encoding a dehydrogenase, was recognised to be responsible for the oxidative function necessary to transform an oxazoline into an oxazole (personal communication D.M, N.Z.). Since, neither the related BGC nor the genetic environment surrounding contained a homologue of *sagB*, we predicted that terpenibactins bear a 2-hydroxyphenyl-5-methyloxazoline residue. Subsequently, the peptide backbone is extended through the condensation of *N*<sup>ε</sup>-formyl-*N*<sup>ε</sup>-hydroxy-L-lysine by the NRPS TerD. Since Thomas and co-workers demonstrated that the A domain of a close homologue of TerD is specific for *N*<sup>ε</sup>-acyl-*N*<sup>ε</sup>-hydroxy-L-lysine,<sup>[34]</sup> the tailoring of the lysine residue by the lysine-*N*-oxygenase TerG and the lysine formyltransferase TerH occurs prior to their insertion into the nocobactin skeleton. The additional C domain within the NRPS *terD* is predicted to condense a 3-hydroxy-2-methyl fatty acid unit into the growing skeleton. The polyketide synthases TerB and TerC are expected to work in conjunction to incorporate the fatty acid into the biosynthesis. Due to the fact that fatty acids of this length cannot be synthesised by a single type I PKS module, it is hypothesised that TerC can select and carry long-chain fatty acids.<sup>[33]</sup> Since the biosynthesis utilises fatty acids from primary metabolism, it is typically challenging to predict the lengths of the acyl chains on the basis of information gleaned from bioinformatics alone; however, considering the range of the nocobactin compound family (Table 1), we assumed the precedence of fatty acid chains between C<sub>7</sub>–C<sub>17</sub> units long. Finally, the NRPS TerE then serves to epimerise and condense a

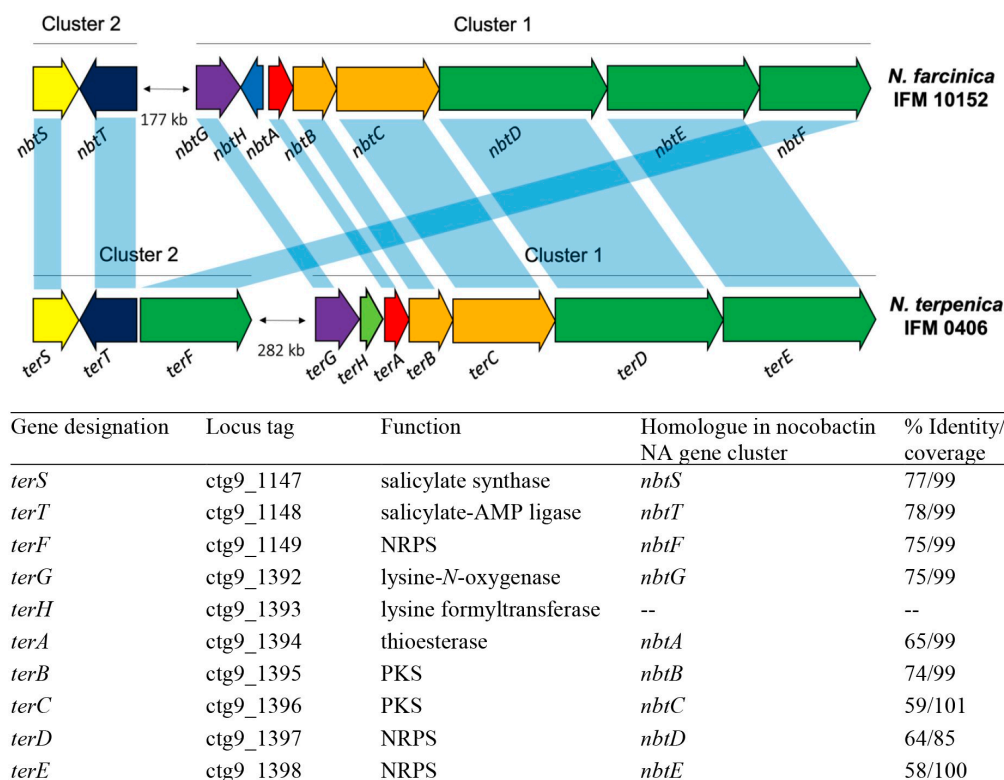


Figure 1. Comparison of the biosynthetic gene clusters encoding (top) nocobactin NA and (bottom) novel terpenibactins.

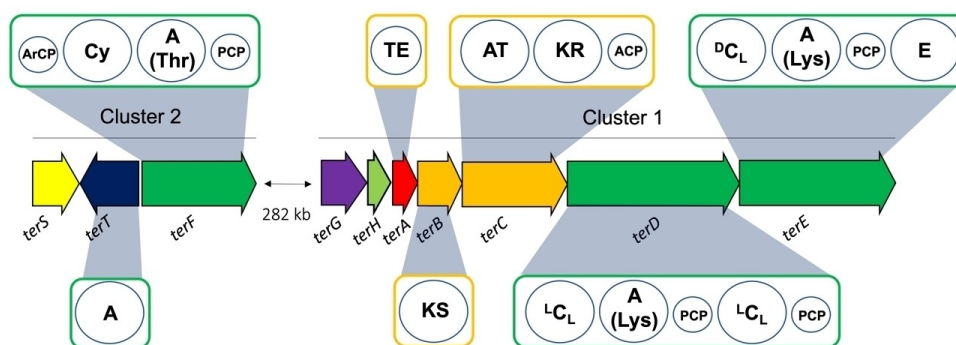


Figure 2. Detailed view of PKS (orange boxes) and NRPS (green boxes) modules in the terpenibactin gene cluster of *N. terpenica* IFM 0406, including A domain substrate specificities.

*N*-hydroxy-lysine residue, which is subsequently lactamised, most likely in a non-enzymatic way.<sup>[35]</sup>

In conclusion, the newly identified gene cluster in strain IFM 0406 was predicted to produce nocobactin-like compounds with  $R^1=R^5=OH$ ,  $R^2=R^4=R^6=R^8=R^9=H$ ,  $R^7=CH_3$  and  $R^3$  ranging from  $C_7H_{15}$  to  $C_{17}H_{35}$ . With these substituents, the resultant compounds should give rise to a suggested mass between 703 and 844 Da. The predicted compounds most closely resemble brasilibactin A or nocardimicins G–I (Table 1), but bear a methyl-oxazoline instead of an oxazoline ring system. The finding that *terF* codes for a threonine-specific A domain that leads, in combination with the absence of *sagB*, to the formation of a methyl-oxazoline ring system, was pivotal.

This fact enabled us to conclude that, regardless of the length of the lipid side chain, the *ter* BGC had to give rise to production of one or more new nocobactin-like compound(s).

#### LC/MS screening for the products of the terpenibactin (*ter*) gene cluster

Methanol extracts of *N. terpenica* IFM 0406 cell pellets were tested for the presence of nocobactin derivatives. A similar strategy was adopted to that used in the isolation of nocobactin NA and similar compounds.<sup>[25–30]</sup> It was intended that extracts would be monitored for compounds in the mass range of 703–

844 Da by use of low-resolution (LR)-LC/MS. The use of chrome azurol S (CAS) assays<sup>[36]</sup> to detect the siderophore of interest proved inapplicable in this isolation effort, given that control extracts of rich, orange-coloured production medium generated false-positive CAS results. Foreseeing the possibility that any secreted siderophores might be complexed with iron at the point of analysis, and knowing from previous literature that ferric nocobactin NA has an absorbance maximum at around 470 nm, extracts were also monitored at this wavelength in HPLC analysis, in addition to the expected maxima produced by the free ligand of 210, 260 and 310 nm.<sup>[25]</sup>

Analysis of cell pellet methanol extracts via LR-LC/MS led to the detection of three peaks with absorbance at 460 nm and masses within the range anticipated for the sought-after compounds ( $M=815.8$ , 841.9 and 843.8 Da). Each compound was detected as their singly charged  $[M+H]^+$  pseudomolecular ion along with their ferrated form  $[M-3H+Fe^{3+}+H]^+$  and the sodium adduct  $[M-3H+Fe^{3+}+Na]^+$  of the latter (see Figures S1 and S2 in the Supporting Information). In summary, the MS data did not match any known compound from the nocobactin family (Table 1) and therefore suggested that IFM 0406 produced at least three new siderophores, which were given the trivial names terpenibactin A (1), B (2) and C (3).

### Isolation and structure elucidation of terpenibactins A–C

To obtain sufficient material to support structural characterization, a 1 L fermentation was performed. Fractionation and purification of the MeOH extract of the cell pellet was carried out by both reversed-phase (RP) vacuum liquid chromatography (VLC) and RP-HPLC. In this way, compounds 1–3 were obtained in a ferrated form (Figure S3). However, due to paramagnetic iron's interference with the magnetic field, which leads to peak broadening and poorly resolved NMR spectra, complete iron removal was necessary in order to perform structure elucidation. Since the method originally described by Ratledge and Snow for full decomplexation of ferric nocobactin<sup>[25]</sup> proved to be inefficient in our hands, we converted the ferric forms of 1–3 into their corresponding

gallium salts and re-purified them by employing HPLC (Figures S4 and S5).<sup>[37,38]</sup>

The analysis of the Ga<sup>III</sup> adduct of terpenibactin A (1) by HR-ESI-MS determined its exact mass to be  $m/z$  882.4156, consistent with the molecular formula  $C_{43}H_{67}GaN_5O_{10}$  ( $\Delta$  1.4 ppm), indicating a structure with 12 degrees of unsaturation. The IR spectrum (Figure S6) possessed absorptions for ester (1738  $cm^{-1}$ ) and amide (1672  $cm^{-1}$ ) carbonyl groups and an aromatic ring system (1617, 1464, 857, 757, 699  $cm^{-1}$ ). UV maxima observed at 219 and 255 and 339 nm (Figure S7) were indicative of a substituted benzenoid chromophore with an extended conjugated system. In the  $^{13}C$  and DEPT135 NMR spectra (Figures S10 and S11), signals assignable to 43 carbons were detected, including those for seven quaternary carbons, one *N*-formyl ( $\delta$  155.3,  $^1J_{C,H}=209$  Hz), four  $sp^2$  methines, six  $sp^3$  methines, 22 methylenes and three methyl groups (Table 2). These data also revealed the presence of nine double bonds ( $3\times CC$ ,  $1\times CN$ ,  $5\times CO$ ); thus, 1 was found to be tricyclic. Analysis of the  $^1H,^1H$  COSY and  $^1H,^{13}C$  HSQC-TOCSY spectrum resolved the partial structures A–E (Figure 3), which were connected by using  $^1H,^{13}C$  HMBC and  $^1H,^1H$  NOESY correlations (Figures S13–S16).

The  $^1H,^1H$  connectivities from H-3 to H-6 and their  $^1H$  and  $^{13}C$  chemical shifts in combination with the  $^1H,^1H$  coupling pattern indicated the presence of a 1,2-disubstituted benzene ring. The chemical shift of C-2 ( $\delta$  167.5) and  $^1H,^{13}C$  HMBC cross correlations between H-3/C-1, H-4/C-2 and H-5/C-1 showed that fragment A consisted of a benzene ring that was substituted with a phenolic hydroxyl group at C-2. The  $^{13}C$  NMR chemical shifts for C-7, C-9, and C-10, together with the doublet proton resonance at  $\delta$  1.49 (H-13), as well as the long-range CH couplings observed between H-10/C-7, H-10/C-12 and H-9/C-12, were all indicative of the presence of a methyl-dihydrooxazole carboxylic acid moiety, which represents fragment B. A long-range CH coupling between H-6 and C-7 allowed the connectivity between C-1 to C-7, and thus that between fragment A and B, to give 9,10-dihydro-asteroidic acid. The typical  $^1H$  and  $^{13}C$  chemical shifts, together with the connected spin system, identified fragment C as a lysine residue.  $^1H,^{13}C$  HMBC long-range correlations between its  $\alpha$ -proton and Lys1-

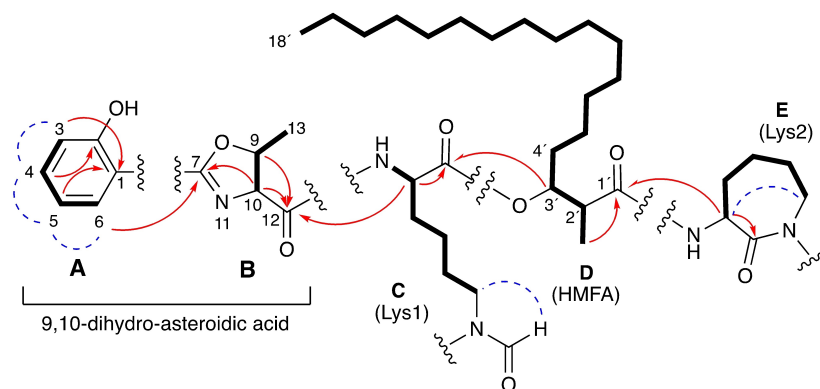


**Figure 3.**  $^1H,^1H$  COSY and  $^1H,^{13}C$  HSQC-TOCSY (bold lines), selected  $^1H,^{13}C$  long-range (red arrows) and selected  $^1H,^1H$  NOESY (dashed blue lines) correlations for terpenibactin A (1). HMFA: hydroxymethyl fatty acid.

**Table 2.** <sup>1</sup>H and <sup>13</sup>C NMR spectroscopic data for terpenibactins A–C (1–3).<sup>[a]</sup>

Atom	Terpenibactin A (1) <sup>[b]</sup>	$\delta_{\text{C}}^{[c]}$	Terpenibactin B (2) <sup>[b]</sup>	$\delta_{\text{C}}^{[c]}$	Terpenibactin C (3) <sup>[b]</sup>	$\delta_{\text{C}}^{[c]}$
9,10-Dihydro-asteroidic acid						
1		110.5, qC		110.5, qC		110.5, qC
2		167.5, qC		167.5, qC		167.5, qC
3	6.81, d (8.5)	122.8, CH	6.81, d (8.5)	122.8, CH	6.81, d (8.5)	122.8, CH
4	7.36, ddd (8.7, 7.9, 1.8)	137.0, CH	7.36, ddd (8.7, 7.9, 1.8)	137.0, CH	7.36, ddd (8.7, 7.9, 1.8)	137.0, CH
5	6.68, t (7.6)	117.3, CH	6.68, t (7.6)	117.3, CH	6.68, t (7.6)	117.3, CH
6	7.67, dd (8.1, 1.8)	130.8, CH	7.67, dd (8.1, 1.8)	130.8, CH	7.67, dd (8.1, 1.8)	130.8, CH
7		171.89, qC <sup>[d]</sup>		171.89, qC <sup>[d]</sup>		171.89, qC <sup>[d]</sup>
9	5.27, dd (5.1, 6.3)	81.0, CH	5.27, dd (5.1, 6.3)	81.0, CH	5.27, dd (5.1, 6.3)	81.0, CH
10	4.31, d (5.1)	73.2, CH	4.31, d (5.1)	73.2, CH	4.30, d (5.2)	73.2, CH
12		170.8, qC		170.8, qC		170.8, qC
13	1.49, d (6.3)	21.3, CH <sub>3</sub>	1.49, d (6.3)	21.3, CH <sub>3</sub>	1.49, d (6.3)	21.3, CH <sub>3</sub>
Lys1						
C=O		171.95, qC <sup>[d]</sup>		171.96, qC <sup>[d]</sup>		171.95, qC <sup>[d]</sup>
$\alpha$	4.39, m	54.9, CH [54.8]	4.39, m	54.9, CH	4.39, m	54.9, CH [54.8]
$\beta$	2.10, m	27.5, CH <sub>2</sub>	2.10, m	27.5, CH <sub>2</sub>	2.10, m	27.5, CH <sub>2</sub>
$\gamma$	1.60, m	19.7, CH <sub>2</sub>	1.60, m	19.7, CH <sub>2</sub>	1.60, m	19.7, CH <sub>2</sub>
	1.97, m		1.97, m		1.97, m	
$\delta$	1.89, m	29.9, CH <sub>2</sub>	1.89, m	29.9, CH <sub>2</sub>	1.89, m	29.9, CH <sub>2</sub>
$\epsilon$	3.70, m	49.5, CH <sub>2</sub>	3.70, m	49.5, CH <sub>2</sub>	3.70, m	49.5, CH <sub>2</sub>
	3.95, m		3.95, m		3.95, m	
NH	9.21, d (4.7)		9.20, d (4.7)		9.21, d (4.7)	
N <sup>F</sup> -CH=O	8.13, s	155.3, CHO		155.3, CHO		155.3, CHO
Hydroxymethyl fatty acid						
1'		173.8, qC [173.9]		173.8, qC		173.8, qC [173.9]
2'	2.62, m	45.26, CH [45.31]	2.62, m	45.3, CH	2.62, m	45.26, CH [45.31]
3'	5.11, dt (2.0, 10.0)	78.0, CH	5.11, dt (2.0, 10.0)	78.0, CH	5.11, dt (2.0, 10.0)	78.0, CH
4'	1.49, m	30.2, CH <sub>2</sub>	1.49, m	30.2, CH <sub>2</sub>	1.49, m	30.2, CH <sub>2</sub>
5'	1.21, m	26.9, CH <sub>2</sub>	2.04, m	28.2, CH <sub>2</sub>	1.21, m	26.9, CH <sub>2</sub>
6'	1.30, m	30.6, CH <sub>2</sub>	5.35, t (4.5)	130.8, CH	1.30, m	30.6, CH <sub>2</sub>
7'	1.30, m	30.6, CH <sub>2</sub>	5.35, t (4.5)	130.8, CH	1.30, m	30.6, CH <sub>2</sub>
8'	1.30, m	30.6, CH <sub>2</sub>	2.04, m	28.2, CH <sub>2</sub>	1.30, m	30.6, CH <sub>2</sub>
9'	1.30, m	30.6, CH <sub>2</sub>	1.30, m	30.6, CH <sub>2</sub>	1.30, m	30.6, CH <sub>2</sub>
10'	1.30, m	30.6, CH <sub>2</sub>	1.30, m	30.6, CH <sub>2</sub>	1.30, m	30.6, CH <sub>2</sub>
11'	1.30, m	30.6, CH <sub>2</sub>	1.30, m	30.6, CH <sub>2</sub>	1.30, m	30.6, CH <sub>2</sub>
12'	1.30, m	30.6, CH <sub>2</sub>	1.30, m	30.6, CH <sub>2</sub>	1.30, m	30.6, CH <sub>2</sub>
13'	1.30, m	30.6, CH <sub>2</sub>	1.30, m	30.6, CH <sub>2</sub>	1.30, m	30.6, CH <sub>2</sub>
14'	1.30, m	30.6, CH <sub>2</sub>	1.30, m	30.6, CH <sub>2</sub>	1.30, m	30.6, CH <sub>2</sub>
15'	1.30, m	30.6, CH <sub>2</sub>	1.30, m	30.6, CH <sub>2</sub>	1.30, m	30.6, CH <sub>2</sub>
16'	1.30, m	33.1, CH <sub>2</sub>	1.30, m	30.6, CH <sub>2</sub>	1.30, m	30.6, CH <sub>2</sub>
17'	1.32, m	23.7, CH <sub>2</sub>	1.30, m	30.6, CH <sub>2</sub>	1.30, m	33.1, CH <sub>2</sub>
18'	0.92, br t (6.9)	14.5, CH <sub>3</sub>	1.30, m	33.1, CH <sub>2</sub>	1.32, m	23.7, CH <sub>2</sub>
19'			1.32, m	23.7, CH <sub>2</sub>	1.30, m	30.6, CH <sub>2</sub>
20'			0.92, br t (6.9)	14.5, CH <sub>3</sub>	0.92, br t (6.9)	14.5, CH <sub>3</sub>
2'-Me	1.14, d (7.2)	14.2, CH <sub>3</sub>	1.14, d (7.3)	14.2, CH <sub>3</sub>	1.14, d (7.2)	14.2, CH <sub>3</sub>
Lys2						
C=O		166.4, qC		166.4, qC		166.4, qC
$\alpha$	4.79, m	51.2, CH [51.3]	4.79, m	51.2, CH	4.79, m	51.2, CH [51.3]
$\beta$	1.48, m	31.68, CH <sub>2</sub> [31.70]	1.48, m	31.7, CH <sub>2</sub>	1.48, m	31.68, CH <sub>2</sub> [31.70]
	1.95, m		1.95, m		1.95, m	
$\gamma$	2.05, m	28.9, CH <sub>2</sub>	2.05, m	28.9, CH <sub>2</sub>	2.05, m	28.9, CH <sub>2</sub>
$\delta$	1.80, m	25.6, CH <sub>2</sub>	1.80, m	25.6, CH <sub>2</sub>	1.80, m	25.6, CH <sub>2</sub>
$\epsilon$	3.85, m	54.4, CH <sub>2</sub>	3.85, m	54.4, CH <sub>2</sub>	3.85, m	54.4, CH <sub>2</sub>
	3.99, m		3.99, m		3.99, m	
NH	n. o. <sup>[e]</sup>		n. o. <sup>[e]</sup>		n. o. <sup>[e]</sup>	
N <sup>F</sup> -C=O		155.3, qC		155.3, qC		155.3, qC

[a] Measured at 400 (<sup>1</sup>H) and 100 MHz (<sup>13</sup>C) in *d*<sub>4</sub>-MeOH. [b] Coupling constants (*J*) are in parentheses and reported in Hz; chemical shifts are given in ppm. [c] Multiplicities were deduced from DEPT135 and multiplicity edited <sup>1</sup>H,<sup>13</sup>C HSQC NMR experiments. <sup>13</sup>C NMR shift values in squared brackets represent a minor conformer (ratio 3:1). [d] Assignments within a column may be interchanged. [e] n.o.: not observed.

CO, and  $^1\text{H},^1\text{H}$  NOESY through-space interactions between the  $\epsilon$ -methylene protons and the formyl hydrogen, defined the complete moiety as *N*-formyl-Lys1. In a similar fashion, fragment E was established as a second lysine residue (Lys2). However, the observation of a correlation between the  $\alpha$ -proton and the corresponding the  $\epsilon$ -methylene protons in the  $^1\text{H},^1\text{H}$  NOESY spectrum indicated that Lys2 was cyclic, hence forming an  $\epsilon$ -aminocaprolactam ring.

The last major fragment, D, was deduced as 2-methyl-3-hydroxyoctadecanoic acid on the basis of the analysis of COSY and HSQC-TOCSY spectra, together with the  $^1\text{H},^{13}\text{C}$  long-range couplings from both H-2' and its 2'-methyl hydrogens to C-1'. The length of the alkyl chain was corroborated by ESI-MS/MS fragment ions. The connectivity of fragment D and E via Lys2-NH resulted from cross peaks in the HMBC spectrum between the  $\alpha$ -proton of Lys2 and C-1'. Coupling between H-3' and Lys1-CO placed partial structure D adjacent to C through an ester bond. Furthermore, the  $\alpha$ -proton of Lys1 exhibited HMBC couplings to C-12, which allowed the connection of partial structure C to B through an amide bond. Taking the molecular formula of 1 into consideration, the remaining two hydroxyl groups were assigned to substituents at the  $\epsilon$ -nitrogen atoms of each lysine residue. This deduction was also supported by MS/MS fragment ions at  $m/z$  145 and 423 (Figure S17). With the planar structure of 1 determined, the configuration at C-2', C-3', C-9, C-10 and the lysine residues required elucidation.

The absolute configuration of the amino acid-related moieties was inferred *in silico* from the BGC. In an NRPS context, the epimerization (E) domains and combined condensation/epimerization (C/E) domains determine the absolute configuration during the biosynthesis process. An E domain was identified in TerE, thus indicating conversion of the activated amino acid Lys2 into the D-configuration. The absence of C/E and E domains in the nonribosomal peptide synthetases TerF and TerD suggests the incorporation and processing of L-configured Thr and Lys1 moieties. In conclusion, from bioinformatics, the stereochemistry was predicted as 10*S*, 9*R*, L-(*S*)-Lys1 and D-(*R*)-Lys2. Concerning the lysine residues, these findings are in agreement with the absolute configuration determined for nocobactin NA. The relative stereochemistry at C-2'-C-3' of the 2-methyl-3-hydroxyoctadecanoic acid was assigned as *erythro* on the basis of the high similarity of  $^1\text{H}$  and  $^{13}\text{C}$  NMR shifts and  $J_{\text{H,H}}$  values between 1 and brasilibactin A. Thus, the structure of terpenibactin A was elucidated to be 1 as shown in Figure 4. With these features, terpenibactin A (1) is most closely related to nocardimicin H, but bears a methyl group instead of a hydrogen atom at R<sup>7</sup> (Figure 4 and Table 1).

Terpenibactin B (2) gave a quasi-molecular ion [ $M-3\text{H} + \text{Ga}^{3+} + \text{H}$ ]<sup>+</sup> at  $m/z$  908.4335 in the HR-ESI-MS, appropriate for the molecular formula  $\text{C}_{45}\text{H}_{69}\text{GaN}_5\text{O}_{10}$  ( $\Delta$  3.8 ppm) and corresponding to 13 degrees of unsaturation. Thus, terpenibactin B (2) differs from terpenibactin A (1) by a  $\text{C}_2\text{H}_2$  group and an additional double bond equivalent. The  $^1\text{H}$  and  $^{13}\text{C}$  NMR spectra of 2 were highly similar to those of 1. However, the  $^{13}\text{C}$  NMR in particular showed elevated signal intensity in the double bond region at  $\delta_{\text{C}}$  130.9 and additional, heightened resonances at  $\delta_{\text{C}}$  28.2. Since both resonances integrated for two carbons, it was

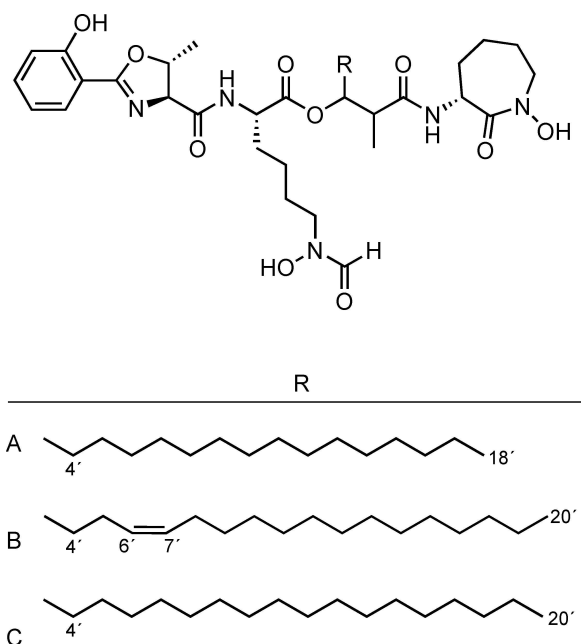


Figure 4. Chemical structures of terpenibactins A–C.

hypothesised that 2 constitutes a double bond between two magnetically equivalent carbon atoms. The HSQC-TOCSY NMR experiment proved that both resonances were part of the spin system of the hydroxymethyl fatty acid of 2. Detailed analysis of the  $^1\text{H},^1\text{H}$  COSY and CH long-range correlations enabled the assignment of  $\Delta^{6,7}$  double bond in 2. Its olefinic coupling constant ( $^3J_{\text{H,H}} = 4.5$  Hz) showed that  $\Delta^{6,7}$  has *Z* geometry. For biogenetic reasons, the same absolute configuration, as given in 1, is suggested for the remaining chiral centres of 2. Terpenibactin B (2) thus most closely resembles nocardimicin I. However, by comparison, 2 bears a methyl group at R<sup>7</sup> of the oxazoline ring system and a double bond in the lipid side chain R<sup>3</sup> (Figure 4 and Table 1).

The molecular formula of terpenibactin C (3) was established as  $\text{C}_{45}\text{H}_{71}\text{GaN}_5\text{O}_{10}$  on the basis of HR-ESI-MS. The  $^1\text{H}$  and  $^{13}\text{C}$  NMR spectra were virtually identical with those of terpenibactin A(1). The MS/MS fragmentation pattern of 3 readily unveiled that the mass shift of 28 mass units (2 methylenes) is attributable to a difference in length of the incorporated fatty acid. Thus, 3 possesses a 2-methyl-3-hydroxyeicosanoic acid moiety instead of a 2-methyl-3-hydroxyoctadecanoic acid in 1. Consequently, terpenibactin C represents a highly similar congener of nocardimicin I, but 3 possesses a methyl-oxazoline instead of an oxazoline ring system (Figure 4 and Table 1).

### Biological properties of terpenibactins A–C

As several nocobactins have shown outstanding antimicrobial,<sup>[28]</sup> cytotoxic<sup>[25,28]</sup> and highly selective muscarinic M3 receptor inhibitory<sup>[29,30]</sup> properties, we evaluated the gallium

(III)-chelated terpenibactins A–C (1–3) in corresponding assays. In standardised antimicrobial assays by broth microdilutions,<sup>[39]</sup> compounds 1–3 were all inactive up to the highest concentration tested (64 µg/mL), while in a cytotoxicity assay using HeLa cells, the compounds exhibited moderate bioactivity. By contrast, all three compounds showed potent muscarinic M3 receptor inhibitory activity, with IC<sub>50</sub> values ranging from 1.15 to 1.77 µM (Table 3). The latter results are in good agreement with the IC<sub>50</sub> values reported for the structurally related nocardimicins A–H, which ranged from 0.37 to 5.89 µM.<sup>[29,30]</sup> Sakagami and co-workers demonstrated that iron(III)-chelated nocobactins exhibit cytotoxic activity that is two orders lower than of the corresponding iron-free forms.<sup>[25]</sup> It is conceivable that the gallium-chelated terpenibactins A–C are affected in a similar fashion, which could explain why compounds 1–3 were found to be inactive in the antimicrobial assay and only moderately active in the cytotoxicity assay.

## Conclusion

Using a bioinformatics approach, we initially deduced already from the *in silico* analysis that the resultant secondary metabolite is new and confirmed the prediction by spectroscopic means. Considering the large number of nocobactins, terpenibactins represent another example of Nature's aptitude in combinatorial chemistry, that is, in this case, through the natural diversification of molecules simply by modification of A-domain substrate specificity, C-domain promiscuity and the presence of dehydrogenases or the efficacy of hydroxylation enzymes. Furthermore, we confirmed the antimuscarinic effect of this compound class, which was already reported for nocardimicins. The addition of terpenibactins to the compound family allowed us to deduce that the antimuscarinic effect of nocobactins appears not to be influenced by the change of the oxidation status of the oxazoline ring, neither by the methylation (serine vs. threonine incorporation) nor by the type of N<sup>ε</sup>-acylation (formylation vs. acetylation). Together with the M3-receptor subtype specificity, found with the nocardimicins, and the moderate cytotoxicity, nocobactins possibly represent an interesting pharmacophore for the development of M3-receptor selective muscarinic inhibitors.

## Experimental Section

**General procedures:** Optical rotation values were measured on a Jasco P-2000 polarimeter, using a 3.5 mm × 10 mm cylindrical

quartz cell. UV spectra were recorded on a PerkinElmer Lambda 25 UV/Vis spectrometer. Infrared spectra were obtained by employing a Jasco FTIR 4200 spectrometer, interfaced with a MIRacle ATR device (ZnSe crystal). HPLC was performed with a Waters system comprising a Waters 1525 binary pump with a 7725i Rheodyne injection port, a Kromega solvent degasser and a Waters 996 photodiode array detector. For low-resolution LC/MS analysis, an 1100 Series HPLC system (Agilent Technologies) was fitted with a G1322 A degasser, a G1312 A binary pump, a G1329 A autosampler, and a G1315 A diode array detector. The Agilent HPLC components were connected with an ABSCIEX 3200 Q TRAP LC/MS/MS mass spectrometer (Sciex, Darmstadt, Germany). 1D and 2D NMR spectra were measured on a Bruker Avance II 400 HD spectrometer using a 5 mm SMART probe head. All NMR spectra were recorded in d<sub>4</sub>-MeOH, processed with TopSpin 3.5 and MestReNova 12.0.4 and calibrated to the residual solvent signals (δ<sub>H/C</sub> 3.31/49.0). High-resolution mass spectra were acquired on an HR-ESI-TOF-MS maXis 4G mass spectrometer (Bruker). All solvents were purchased as HPLC or LC/MS grade. Chemicals were purchased from Sigma-Aldrich or VWR. Steam sterilization of medium components and waste were performed at 121 °C for 15 min at 2.1 bar using a Systec VX-150 autoclave, equipped with air exhaust filtration.

**Bacterial material and cultivation conditions:** The producer strain *N. terpenica* IFM 0406 was purchased from the culture collection of the Medical Mycology Research Center (MMRC), Chiba University, Chiba, Japan. For cultivation, a protocol conceived by Ikeda et al.<sup>[29a]</sup> was adapted. 100 mL of preculture medium (consisting of 10 g/L soluble starch, 5 g/L glucose, 3 g/L NZ-case, 2 g/L yeast extract, 5 g/L tryptone, 1 g/L K<sub>2</sub>HPO<sub>4</sub>, 0.5 g/L MgSO<sub>4</sub> and 3 g/L CaCO<sub>3</sub>, adjusted to pH 7.0 before sterilization) in a 500 mL baffled Erlenmeyer flask was inoculated with a loopful of a 3-day-old agar culture of the strain, and shaken at 150 rpm at 37 °C for five days, using an INFORS HT Multitron Pro orbital incubator shaker. 3 mL of this culture was in turn used to inoculate 200 mL volumes of production medium (consisting of 5 g/L glucose, 20 g/L glycerol, 20 g/L soluble starch, 15 g/L Pharmamedia and 3 g/L yeast extract, adjusted to pH 7.0 before sterilization) in 500 mL Erlenmeyer flasks. Fermentation was carried out at 30 °C at 150 rpm for five days.

**LC/MS screening:** Following small scale cultivation (200 mL), cultures were centrifuged in a Thermo Scientific Heraeus Multifuge 4KR centrifuge at 5346 g for 10 min. Subsequently, the supernatant was extracted with ethyl acetate (1:1), while the cell pellet was extracted with 200 mL methanol. Upon evaporation of each extract under reduced pressure, the resultant crude extracts of each experiment were dissolved in methanol with a few drops of water, centrifuged to remove detritus prior to analysis, and profiled by LC/MS using a MeOH/H<sub>2</sub>O gradient, increasing the MeOH portion from 50 to 100% over 20 min, followed by isocratic elution at 100% MeOH for an additional 20 min (Phenomenex Luna C18 (2)–100 Å column, 250 × 2.0 mm, 5 µm; 0.2 mL/min flow rate; with total ion current [Q3 MS positive scan mode] and photodiode array monitoring). The following MS parameters were used for this analysis: declustering potential: 70 V; entrance potential: 10 V; curtain gas: 10 psi; collision gas: 2 psi; ion spray source voltage: 4500 V; additional temperature: 450 °C, ion source gas 1 (nebuliser gas): 50 psi; ion source gas 2 (drying gas): 50 psi.

**Isolation and extraction:** All the broth from a 1 L fermentation of IFM 0406 was centrifuged, the cell pellet extracted with 6 × 200 mL MeOH, and evaporated to dryness. The cell pellet extract was resuspended and further fractionated via vacuum liquid chromatography (VLC). The reversed-phase (RP) C<sub>18</sub> column (dimensions: 10 × 5 cm; material: Macherey-Nagel Polygoprep 50–60 C<sub>18</sub> RP silica gel) was eluted stepwise under vacuum with solvents of decreasing polarity (300 mL per fraction), ranging from a 50:50 MeOH/H<sub>2</sub>O mixture to pure methanol, followed by 100% dichloromethane to

Compound	Muscarinic M3 receptor inhibitory activity IC <sub>50</sub>	Cytotoxicity IC <sub>50</sub> (HeLa)
terpenibactin A (1)	1.15 ± 0.13 µM	16.7 µg/mL
terpenibactin B (2)	1.77 ± 0.26 µM	45.9 µg/mL
terpenibactin C (3)	1.59 ± 0.13 µM	33.3 µg/mL
atropine	8.10 ± 0.80 nM	N/A

give seven fractions (A–G). Fraction G, eluting with 100% dichloromethane, was further purified by RP-HPLC using a linear gradient from 50:50 to 100:0 (MeOH/H<sub>2</sub>O) over a period of 10 min, followed by isocratic elution at 100% MeOH for an additional 25 min (Phenomenex Aeris Peptide XB–C18 column, 4.6 × 250 mm, 3.6 μm; 0.6 mL/min flow rate, UV monitoring at 340 and 460 nm), which yielded pure terpenibactins A (13.6 mg), B (10.9 mg) and C (7.4 mg).

**Ga<sup>III</sup>-complex formation:** A suspension of 5 mg gallium sulphate in 30 mL MeOH:H<sub>2</sub>O (1:1) was added to a near-dry fresh methanol pellet extract, and the sample rotated for one hour. This was then evaporated to dryness, resuspended in methanol and analysed using LR-LC/MS. Results showed that three new peaks had formed alongside the ferrated components, with higher intensities and masses corresponding to the gallium-complexed forms of their ferrated neighbours. Notably, repeated LR-LC/MS analysis, two days after the run that first evidenced the formation of gallium complexes, demonstrated that only trace amounts remained of the ferrated forms of the compounds of interest, suggesting a time-dependent complete interconversion of iron to gallium complexes even within a sample dried and stored at –20 °C.

**Chrome azurol S (CAS)-assay:** The CAS assay agar plates for the detection of siderophores were prepared on a 100 mL scale as previously described.<sup>[36]</sup>

**Antibacterial assays:** The minimal inhibitory concentration (MIC) was determined in cation-adjusted Mueller-Hinton medium that contains casein, beef extract and starch by using a twofold serial dilution method according to the standards and guidelines of the Clinical and Laboratory Standards Institute (CLSI).<sup>[39]</sup> In brief, a twofold serial dilution of the test compound was prepared in microtiter plates and seeded using a final test concentration of bacteria of 5 × 10<sup>5</sup> colony-forming units per mL. After the overnight incubation at 37 °C, the MIC was determined as the lowest compound concentration preventing visible bacterial growth. The strain panel included representative species of nosocomial pathogens, which are known as “ESKAPE” bacteria. Specifically, the following strains were used: *Enterococcus faecium* BM 4147–1, *Staphylococcus aureus* ATCC 29213, *Klebsiella pneumoniae* ATCC 12657, *Acinetobacter baumannii* 09987, *Pseudomonas aeruginosa* ATCC 27853 and *Enterobacter aerogenes* ATCC 13048. *Bacillus subtilis* 168 and *Escherichia coli* ATCC 25922 were used as further reference strains. The ATCC strains were provided by the American Type Culture Collection. *A. baumannii* 09987 was obtained from the University of Bonn, Germany.

**Cytotoxicity assay:** The cytotoxicity test against the HeLa human cervical carcinoma cell line was performed in RPMI cell culture medium supplemented with 10% foetal bovine serum using the 7-hydroxy-3H-phenoxazin-3-one-10-oxide (resazurin) assay. A twofold serial dilution of the test compounds was prepared in duplicates in a microtiter plate and seeded with trypsinised HeLa cells to a final cell concentration of 1 × 10<sup>4</sup> cells per well. After 24 h incubation at 37 °C, 5% CO<sub>2</sub>, 95% relative humidity, resazurin was added at a final concentration of 200 μM, and cells were again incubated overnight. Cell viability was assessed by determining the reduction of resazurin to the fluorescent resorufin. Fluorescence was measured in a TECAN M200 reader at an excitation wavelength of 560 nm and an emission wavelength of 600 nm in relation to an untreated control.

**Muscarinic M3 receptor calcium flux assay:** Chem-1 frozen cells, stably transfected with a clone of the human M3 muscarinic acetylcholine receptor (CHRM3 cDNA, HTS116RTA), were purchased from Eurofins Pharma Bioanalytical Services US Inc. They were thawed, suspended and seeded in 96-well plates containing the media component according to the manufacturer's instructions.

The assay plates were then incubated overnight at 37 °C in a 5% CO<sub>2</sub> humidified atmosphere, during which the cell adhered to the bottom of the wells, followed by the removal of media components prior to use in the calcium assay.

Cytosolic-free calcium concentration ([Ca<sup>2+</sup>]<sub>i</sub>) was measured using the calcium mobilization assay with fluorescent dyes. The dye-loading solution containing Fluo-8 NW Ca<sup>2+</sup> dye, 10X Pluronic® F127 Plus and Hanks' buffer with 20 mM HEPES was prepared according to the Screen Quest™ Fluo-8 NW calcium assay kit (AAT Bioquest). Probenecid acid was not applied to this method. At the start of the assay, the 96-well plates containing Chem-1 cells were loaded with an equal volume of dye-loading solutions at 37 °C for 1 h. Afterwards, the cells were pre-incubated with the GPCR-antagonist test compounds terpenibactin A, B, and C for 30 min prior to the injection of the acetylcholine agonist (Sigma) at the final concentration of 250 nM. The final volume was 100 μL per well. The changes in fluorescence intensities in response to the indicated ligand were measured using a Tecan Infinite M200® injection system with a filter set for excitation and emission at 490 and 525 nm, respectively. IC<sub>50</sub> values and associated SEMs were calculated by curve-fitting the relative fluorescence unit data to an sigmoidal model using GraphPad Prism 7.00.

## Acknowledgements

We kindly thank Dr. Wistuba (Mass Spectrometry Department, Institute for Organic Chemistry, University of Tübingen, Germany) for HR-MS measurements and Dr. Luqman (Microbial Genetics Department, Interfaculty Institute of Microbiology and Infection Medicine, University of Tübingen, Germany) for technical assistance in conducting the calcium mobilization assay. A. F. gratefully acknowledges the Program for Research and Innovation in Science and Technology (RISET-Pro)/World Bank Loan No. 8245 for a granted Ph.D. scholarship. H.B.-O., N.Z., L.K. and H.G. gratefully acknowledge support of the Deutsche Forschungsgemeinschaft (DFG, German Research Foundation) – Project ID 398967434-TRR 261.

## Conflict of Interest

The authors declare no conflict of interest.

- [1] E. Nocard, *Ann. Inst. Pasteur* **1888**, *2*, 293–302.
- [2] M. Fatahi-Bafghi, *Microb. Pathog.* **2018**, *114*, 369–384.
- [3] J. W. Wilson, *Mayo Clin. Proc.* **2012**, *87*, 403–407.
- [4] Q. Luo, S. Hiessl, A. Poehlein, R. Daniel, A. Steinbüchel, *Appl. Environ. Microbiol.* **2014**, *80*, 3895–3907.
- [5] K. A. El Sayed, *J. Nat. Prod.* **1998**, *61*, 149–151.
- [6] Z. H. Cheng, B. Y. Yu, G. A. Cordell, S. X. Qiu, *Org. Lett.* **2004**, *6*, 3163–3165.
- [7] D. Dhakal, A. K. Chaudhary, A. R. Pokhrel, A. K. Jha, S. Darsandhari, B. Shrestha, J. K. Sohng, *J. Biomol. Reconstruct.* **2013**, *10*, 9–17.
- [8] D. Dhakal, V. Rayamajhi, R. Mishra, J. K. Sohng, *J. Ind. Microbiol. Biotechnol.* **2019**, *46*, 385–407.
- [9] L. Vera-Cabrera, R. Ortiz-Lopez, R. Elizondo-Gonzalez, J. Ocampo-Candiani, *PLoS One* **2013**, *8*, e65425.
- [10] M. Imajoh, Y. Fukumoto, J. Yamane, M. Sakeda, M. Shimizu, K. Ohnishi, S.-I. Oshima, *Genome* **2015**, *3*, e00082–15.
- [11] F. Vautrin, E. Bergeron, A. Dubost, D. Abrouk, C. Martin, B. Cournoyer, V. Louzier, T. Winiarski, V. Rodriguez-Nava, P. Pujic, *Microbiol. Res.* **2019**, *8*, e00600–19.



- [12] M. A. Schorn, M. M. Alanjary, K. Aguinaldo, A. Korobeynikov, S. Podell, N. Patin, T. Lincecum, P. R. Jensen, N. Ziemert, B. S. Moore, *Microbiology* **2016**, *162*, 2075–2086.
- [13] Y. Hoshino, K. Watanabe, S. Iida, S. Suzuki, T. Kudo, T. Kogure, K. Yazawa, J. Ishikawa, R. M. Kroppenstedt, Y. Mikami, *Int. J. Syst. Evol. Microbiol.* **2007**, *57*, 1456–1460.
- [14] V. Wiebach, A. Mainz, M.-A. J. Siegert, N. A. Jungmann, G. Lesquame, S. Tirat, A. Dreux-Zigha, J. Aszodi, D. Le Beller, R. D. Süßmuth, *Nat. Chem. Biol.* **2018**, *14*, 652–654.
- [15] Y. Tanaka, H. Komaki, K. Yazawa, Y. Mikami, A. Nemoto, T. Tojyo, K. Kadowaki, H. Shigemori, J. Kobayashi, *J. Antibiot.* **1997**, *50*, 1036–1041.
- [16] K. Komatsu, M. Tsuda, Y. Tanaka, Y. Mikami, J. Kobayashi, *J. Org. Chem.* **2004**, *69*, 1535–1541.
- [17] H. T. Chiu, C. P. Weng, Y. C. Lin, K. H. Chen, *Org. Biomol. Chem.* **2016**, *14*, 1988–2006.
- [18] H. Shigemori, H. Komaki, K. Yazawa, Y. Mikami, A. Nemoto, Y. Tanaka, T. Sasaki, Y. In, T. Ishida, J. Kobayashi, *J. Org. Chem.* **1998**, *63*, 6900–6904.
- [19] H. Komaki, A. Nemoto, Y. Tanaka, H. Takagi, K. Yazawa, Y. Mikami, H. Shigemori, J. Kobayashi, A. Ando, Y. Nagata, *J. Antibiot.* **1999**, *52*, 13–19.
- [20] K. Komatsu, M. Tsuda, M. Shiro, Y. Tanaka, Y. Mikami, J. Kobayashi, *Bioorg. Med. Chem.* **2004**, *12*, 5545–5551.
- [21] T. Usui, Y. Nagumo, A. Watanabe, T. Kubota, K. Komatsu, J. Kobayashi, H. Osada, *Chem. Biol.* **2006**, *13*, 1153–1160.
- [22] Y. Hayashi, N. Matsuura, H. Toshima, N. Itoh, J. Ishikawa, Y. Mikami, T. Dairi, *J. Antibiot.* **2008**, *61*, 164–174.
- [23] A. Buchmann, M. Eitel, P. Koch, P. N. Schwarz, E. Stegmann, W. Wohlleben, M. Wolański, M. Krawiec, J. Zakrzewska-Czerwińska, C. Méndez, A. Botas, L. E. Núñez, F. Moris, J. Cortés, H. Gross, *Genome* **2016**, *4*, e01391–16.
- [24] P. N. Schwarz, A. Buchmann, L. Roller, A. Kulik, H. Gross, W. Wohlleben, E. Stegmann, *Biotechnol. J.* **2018**, *13*, 1700527.
- [25] a) C. Rattledge, G. A. Snow, *Biochem. J.* **1974**, *139*, 407–413; b) H. Sakagami, M. Ishihara, Y. Hoshino, J. Ishikawa, Y. Mikami, T. Fukai, *In Vivo* **2005**, *19*, 277–282.
- [26] Y. Murakami, S. Kato, M. Nakajima, M. Matsuoka, H. Kawai, K. Shin-Ya, H. Seto, *J. Antibiot.* **1996**, *49*, 839–845.
- [27] a) K. Suenaga, S. Kokubo, C. Shinohara, T. Tsuji, D. Uemura, *Tetrahedron Lett.* **1999**, *40*, 1945–1948; b) K. Kokubo, K. Suenaga, C. Shinohara, T. Tsuji, D. Uemura, *Tetrahedron* **2000**, *56*, 6435–6440.
- [28] M. Tsuda, M. Yamakawa, S. Oka, Y. Tanaka, Y. Hoshino, Y. Mikami, A. Sato, H. Fujiwara, Y. Ohizumi, J. Kobayashi, *J. Nat. Prod.* **2005**, *68*, 462–464.
- [29] a) Y. Ikeda, H. Nonaka, T. Furumai, H. Onaka, Y. Igarashi, *J. Nat. Prod.* **2005**, *68*, 1061–1065; b) J. C. Banks, C. J. Moody, *Tetrahedron Lett.* **2009**, *50*, 3371–3373.
- [30] Y. Ikeda, T. Furumai, Y. Igarashi, *J. Antibiot.* **2005**, *58*, 566–572.
- [31] K. Blin, S. Shaw, K. Steinke, R. Villebro, N. Ziemert, S. Y. Lee, M. H. Medema, T. Weber, *Nucleic Acids Res.* **2019**, *47*, W81–W87.
- [32] J. Bursy, A. U. Kuhlmann, M. Pittelkow, H. Hartmann, M. Jebbar, A. J. Pierik, E. Bremer, *Appl. Environ. Microbiol.* **2008**, *74*, 7286–7296.
- [33] Y. Hoshino, K. Chiba, K. Ishino, T. Fukai, Y. Igarashi, K. Yazawa, Y. Mikami, J. Ishikawa, *J. Bacteriol.* **2011**, *193*, 441–448.
- [34] M. D. McMahon, J. S. Rush, M. G. Thomas, *J. Bacteriol.* **2012**, *194*, 2809–2818.
- [35] X. Liu, Y. Jin, Z. Cui, K. Nonaka, S. Baba, M. Funabashi, Z. Yang, S. G. Van Lanen, *ChemBioChem* **2016**, *17*, 804–810.
- [36] B. Schwyn, J. B. Neilands, *Anal. Biochem.* **1987**, *160*, 47–56.
- [37] T. Emery, *Biochemistry* **1986**, *25*, 4629–33.
- [38] a) H. Stephan, S. Freund, W. Beck, G. Jung, J. M. Meyer, G. Winkelmann, *BioMetals* **1993**, *6*, 93–100; b) S. Lautru, R. J. Deeth, L. M. Bailey, G. L. Challis, *Nat. Chem. Biol.* **2005**, *1*, 265–269.
- [39] J. B. Patel, F. R. Cockerill, P. A. Bradford, G. M. Eliopoulos, J. A. Hindler, S. G. Jenkins, J. S. Lewis, B. Limbago, L. A. Miller, D. P. Nicolau, M. Powell, J. M. Swenson, J. D. Turnidge, M. P. Weinstein, B. L. Zimmer, *Methods for Dilution Antimicrobial Susceptibility Tests for Bacteria that Grow Aerobically. Approved Standard, Vol. 35*, 10th ed., Clinical and Laboratory Standards Institute, USA, **2015**.

---

Manuscript received: January 31, 2020

Revised manuscript received: March 7, 2020

Accepted manuscript online: March 20, 2020

Version of record online: April 2, 2020